

Reconstructing the history of water ice formation from HDO/H₂O and D₂O/HDO ratios in protostellar cores

K. Furuya¹, E. F. van Dishoeck^{1,2}, and Y. Aikawa³

¹ Leiden Observatory, Leiden University, P.O. Box 9513, 2300 RA, The Netherlands
e-mail: furuya@strw.leidenuniv.nl

² Max-Planck-Institut für Extraterrestrische Physik, Giessenbachstrasse, Garching, Germany

³ Center for Computer Sciences, University of Tsukuba, Tsukuba 305-8577, Japan

Preprint online version: July 30, 2018

ABSTRACT

Recent interferometer observations have found that the D₂O/HDO abundance ratio is higher than that of HDO/H₂O by about one order of magnitude in the vicinity of low-mass protostar NGC 1333-IRAS 2A, where water ice has sublimated. Previous laboratory and theoretical studies show that the D₂O/HDO ice ratio should be lower than the HDO/H₂O ice ratio, if HDO and D₂O ices are formed simultaneously with H₂O ice. In this work, we propose that the observed feature, D₂O/HDO > HDO/H₂O, is a natural consequence of chemical evolution in the early cold stages of low-mass star formation: 1) majority of oxygen is locked up in water ice and other molecules in molecular clouds, where water deuteration is not efficient, and 2) water ice formation continues with much reduced efficiency in cold prestellar/protostellar cores, where deuteration processes are highly enhanced due to the drop of the ortho-para ratio of H₂, the weaker UV radiation field, etc. Using a simple analytical model and gas-ice astrochemical simulations tracing the evolution from the formation of molecular clouds to protostellar cores, we show that the proposed scenario can quantitatively explain the observed HDO/H₂O and D₂O/HDO ratios. We also find that the majority of HDO and D₂O ices are likely formed in cold prestellar/protostellar cores rather than in molecular clouds, where the majority of H₂O ice is formed. This work demonstrates the power of the combination of the HDO/H₂O and D₂O/HDO ratios as a tool to reveal the past history of water ice formation in the early cold stages of star formation and when the enrichment of deuterium in the bulk of water occurred. Further observations are needed to explore if the relation, D₂O/HDO > HDO/H₂O, is common in low-mass protostellar sources.

Key words. astrochemistry — ISM: molecules — ISM: clouds — Stars: protostars

1. Introduction

The degree of deuterium fractionation in molecules in general, and that of water in particular, depends on its formation environments. This characteristic allows us to gain insights into the water trail from its formation in molecular clouds to, ultimately, the delivery to planets by comparing the deuterium fractionation in objects at different evolutionary stages (e.g., recent reviews by Ceccarelli et al., 2014; van Dishoeck et al., 2014).

It is well established that water is formed on grain surfaces in molecule clouds. At dust temperatures lower than 100-150 K, water is predominantly present on the surfaces of dust grains as ice (Fraser et al., 2001). There has been no clear detection of HDO ice in the interstellar medium (ISM), and the deuteration of water ice is not well-constrained ($\text{HDO}/\text{H}_2\text{O} < (2 - 5) \times 10^{-3}$; Dartois et al., 2003; Parise et al., 2003). Instead, there have been numerous observational studies on the deuteration of water vapor, which may reflect that of water ice through thermal and non-thermal desorption of ice.

In particular, recent interferometer and single-dish observations have quantified the degree of deuteration of water vapor in four low-mass protostellar sources, IRAS 16293-2422, NGC 1333-IRAS 2A, IRAS 4A, and IRAS 4B (Jørgensen & van Dishoeck, 2010; Liu et al., 2011; Coutens et al., 2012, 2013, 2014; Persson et al., 2013, 2014; Taquet et al., 2013). The interferometer observations provide the emission from the inner hot regions ($T > 100$ K), where water ice is sublimated, while the single-dish observations including

the *Herschel* Space Observatory provide the integrated emission from larger spacial scales (Jørgensen & van Dishoeck, 2010; Coutens et al., 2012). The combination of the two types of the observations have revealed that 1) the gaseous HDO/H₂O ratio in the inner hot regions ($\sim 10^{-3}$) is lower than that in the cold outer envelopes by more than one order of magnitude, and 2) the gaseous D₂O/HDO ratio is much higher than the HDO/H₂O ratio ($\sim 10^{-2}$ versus $\sim 10^{-3}$) in the inner hot regions of NGC 1333-IRAS 2A (Coutens et al., 2014) and at least one other source (A. Coutens 2015, private communication).

Water deuteration in low-mass protostellar sources has also been studied using physical and astrochemical models (e.g., recent work by Aikawa et al., 2012; Taquet et al., 2014; Wakelam et al., 2014). These studies adopt one-dimensional gravitational collapse models, which describe the physical evolution of collapsing prestellar cores to protostellar sources, with detailed gas-ice chemical networks. The models successfully reproduce observed feature #1, the radial gradient of the HDO/H₂O ratio, by gas-phase ion-neutral chemistry in the outer cold regions and sublimation of ice in the inner hot regions. The models, however, tend to overpredict the HDO/H₂O ratio in the inner hot regions by a factor of several or more compared to the observations. Furthermore, in contrast to the observed feature #2, all models predict that the gaseous D₂O/HDO ratio in the inner hot regions is lower than or comparable to the HDO/H₂O ratio. Coutens et al. (2014) have proposed that either there is something missing in the current understanding of deuterium

chemistry on icy grain surfaces, or that water formation at high temperatures ($T_{\text{gas}} > 200\text{--}300$ K) through reactions $\text{O} + \text{H}_2 \rightarrow \text{OH} + \text{H}$ and $\text{OH} + \text{H}_2 \rightarrow \text{H}_2\text{O} + \text{H}$ play a role in the inner quiescent regions, following sublimation of ice. In the latter case, the $\text{D}_2\text{O}/\text{HDO}$ ratio reflects that in ice, while the $\text{HDO}/\text{H}_2\text{O}$ ratio is diluted by the additional formation of H_2O vapor, so that the $\text{D}_2\text{O}/\text{HDO}$ ratio can be higher than the $\text{HDO}/\text{H}_2\text{O}$ ratio. However, it requires that a large amount of oxygen is in atomic form rather than in molecules in the high density inner regions.

In this paper, we propose an alternative scenario that can account for the higher $\text{D}_2\text{O}/\text{HDO}$ ratio compared with $\text{HDO}/\text{H}_2\text{O}$ by the combination of cold deuterium chemistry and sublimation of ice without the need for the enhanced H_2O formation in hot gas. This paper is organized as follows. In Section 2, the proposed scenario is presented through a simple analytical model. In Section 3, we simulate the gas-ice chemical evolution in star-forming cores with a numerical model to verify the scenario. We briefly discuss molecular oxygen and the ortho-to-para ratio of H_2 , the deuteration of methanol, and thermally induced H-D exchange reactions in ice in Section 4. Our findings are summarized in Section 5.

2. Scenario

We assume that both the $\text{HDO}/\text{H}_2\text{O}$ and $\text{D}_2\text{O}/\text{HDO}$ gas ratios in the inner hot regions around protostars reflect those in ice. In this subsection we denote the $\text{HDO}/\text{H}_2\text{O}$ ratio as f_{D1} , while we denote the $\text{D}_2\text{O}/\text{HDO}$ ratio as f_{D2} .

We first note that previous laboratory and theoretical studies show that f_{D2} should be lower than f_{D1} , if H_2O , HDO , and D_2O ices are formed via grain surface reactions at the same time. Let us assume that they all are formed via sequential reactions of atomic hydrogen/deuterium with atomic oxygen. These reactions have no activation energy barrier (Allen & Robinson, 1977). If the surface reactions distribute deuterium statistically (or, in other words, mass-independently), the following relation holds (Rodgers & Charnley, 2002):

$$[f_{\text{D2}}/f_{\text{D1}}]_{\text{statistic}} = 0.25. \quad (1)$$

Laboratory experiments have demonstrated that there are other formation pathways of water ice: sequential surface reactions initiated by reactions of O_2/O_3 with atomic hydrogen (Ioppolo et al., 2008; Miyauchi et al., 2008; Mokrane et al., 2009), and the reaction $\text{OH} + \text{H}_2 \rightarrow \text{H}_2\text{O} + \text{H}$ (Oba et al., 2012). These pathways include reactions with activation energy barriers, and thus proceed through quantum tunneling (Oba et al., 2012, 2014). The barrier-mediated reactions favor hydrogenation over deuteration, because deuterium is twice heavier than hydrogen (Oba et al., 2014). In addition, once water is formed, it does not efficiently react with atomic deuterium to be deuterated at low temperatures unlike formaldehyde and methanol (Nagaoka et al., 2005). At warm temperatures (>70 K), H-D exchange reaction, $\text{H}_2\text{O} + \text{D}_2\text{O} \rightarrow 2\text{HDO}$, is thermally activated, and the $f_{\text{D2}}/f_{\text{D1}}$ ratio can be lowered (e.g., Lamberts et al., 2015, see also Section 4.3). Taken together, 0.25 is the upper limit of the $f_{\text{D2}}/f_{\text{D1}}$ ratio.

The above constraint, $f_{\text{D2}}/f_{\text{D1}} \leq 0.25$, can be directly applied to the compositions of ice in the ISM, if H_2O , HDO , and D_2O ices are predominantly formed simultaneously (Butner et al., 2007). However, in the sequence of star formation, they are not necessarily formed at the same evolutionary stage (Dartois et al., 2003). The onset of water ice mantle formation requires a threshold extinction, above which the photodesorption rate of water

ice is lower than the formation rate of water ice and its precursors (e.g., Tielens, 2005). The H_2O ice formation rate decreases with time as elemental oxygen is locked into O-bearing molecules. Later in the evolution, at higher extinction and densities, CO freezes out and the products of its hydrogenation, such as formaldehyde (H_2CO) and methanol (CH_3OH), are thought to be the main constituent of the outer layers of the ice mantle (e.g., Pontoppidan, 2006; Öberg et al., 2011). On the other hand, the formation rates of HDO and D_2O ices do not necessarily decrease together with that of H_2O ice; deuterium fractionation is more efficient at later times, as CO is frozen out, the ortho-to-para nuclear spin ratio of H_2 ($\text{OPR}(\text{H}_2)$) decreases, and interstellar UV radiation is heavily shielded (e.g., Caselli & Ceccarelli, 2012, and references therein).

Infrared observations show that H_2O ice starts to become abundant in molecular clouds above a threshold line of sight visual extinction, depending on environments, e.g., ~ 3 mag for Taurus dark clouds (Whittet, 1993; Boogert et al., 2015, and references therein). The scenario we propose is that, in contrast to H_2O ice, HDO and D_2O ices are mainly formed at the later stages of star formation, i.e., in cold prestellar and protostellar cores, where deuterium fractionation processes would be more efficient than in ambient molecular clouds. Then, considering the layered structure of ice mantles, HDO and D_2O are mainly present in the $\text{CO}/\text{CH}_3\text{OH}$ -rich outer layers, rather than the H_2O -dominated inner layers. Assuming complete sublimation of the ice mantles in the inner hot regions of low-mass protostars, the gaseous $\text{D}_2\text{O}/\text{HDO}$ ratio directly reflects that in the outer layers of the ice mantles, while the gaseous $\text{HDO}/\text{H}_2\text{O}$ ratio is much lower than that in the outer layers due to the dilution by the abundant H_2O in the inner layers. Thus, the gaseous $\text{D}_2\text{O}/\text{HDO}$ ratio can be higher than the $\text{HDO}/\text{H}_2\text{O}$ ratio in the vicinity of protostars. A schematic view of the layered ice structure in our scenario is shown in Figure 1. Our scenario is essentially similar to that proposed by Dartois et al. (2003) for HDO enhancement. They suggested that water ice is formed without deuterium enrichment, followed by the additional water formation with high levels of deuterium fractionation at later times. The motivation behind their scenario was to explain the upper limits of the icy $\text{HDO}/\text{H}_2\text{O}$ ratio in the cold outer envelope of protostars, which are lower than the D/H ratios of other gaseous species.

To get a rough idea of how high the $f_{\text{D2}}/f_{\text{D1}}$ ratio can be in our scenario and to investigate the critical parameters, let us consider a two stage model (or a two layer ice model). We denote the total amount of oxygen locked into H_2O , HDO or D_2O ices at each stage (or in each layer) k , where $k = \text{I}$ or II , as $N_{\text{O},k}$. We denote the fraction of oxygen locked into X_2O ice, where X is H or D, as $P_{\text{X}_2\text{O},k}$. Then, $P_{\text{X}_2\text{O},k}N_{\text{O},k}$ represents the amount of X_2O ice formed in the stage k . We can express f_{D1} and f_{D2} in the bulk of ice mantle as follows:

$$[f_{\text{D1}}]_{\text{I+II}} = \frac{\sum_{k=\text{I,II}} P_{\text{HDO},k} N_{\text{O},k}}{\sum_{k=\text{I,II}} P_{\text{H}_2\text{O},k} N_{\text{O},k}}, \quad (2)$$

$$[f_{\text{D2}}]_{\text{I+II}} = \frac{\sum_{k=\text{I,II}} P_{\text{D}_2\text{O},k} N_{\text{O},k}}{\sum_{k=\text{I,II}} P_{\text{HDO},k} N_{\text{O},k}}. \quad (3)$$

It would be reasonable to assume $P_{\text{H}_2\text{O},k} \sim 1$. Motivated by Equation (1), we introduce a free parameter q as $P_{\text{D}_2\text{O},k}/P_{\text{HDO},k} = qP_{\text{HDO},k}/P_{\text{H}_2\text{O},k}$ in the range of $0 < q \leq 0.25$. When $q = 0.25$, deuterium is statistically distributed, i.e., the most optimistic case to obtain a high $f_{\text{D2}}/f_{\text{D1}}$. Although q can vary between the two stages, we assume it is constant for simplicity. With those relations, the $f_{\text{D2}}/f_{\text{D1}}$ ratio in the bulk of the

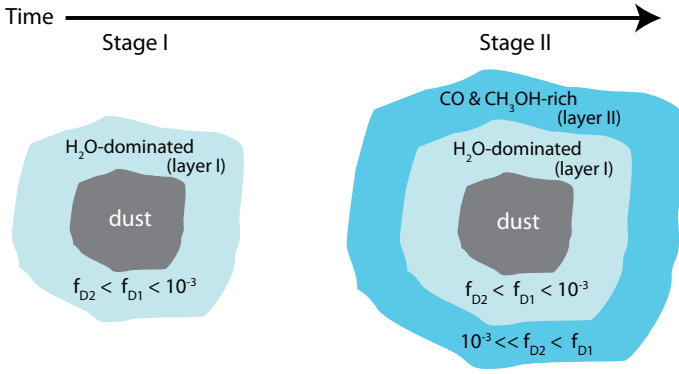


Fig. 1. Schematic view of our scenario and the layered ice structure. Stage I) The main formation stage of H₂O ice. Water deuteration is not efficient, $f_{D2} < f_{D1} < 10^{-3}$. The majority of oxygen is locked in O-bearing molecules in this stage. Stage II) CO/CH₃OH-rich outer ice layers are formed, while the formation of water ice continues with much reduced efficiency compared to Stage I. Nevertheless, the formation of HDO and D₂O ices is more efficient than in Stage I, due to the enhanced deuteration processes, $10^{-3} \ll f_{D2} < f_{D1}$.

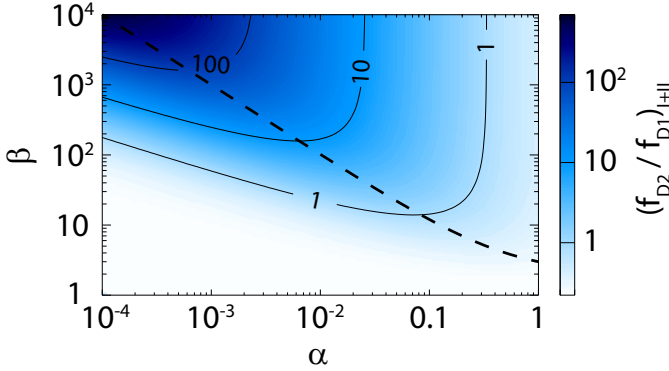


Fig. 2. The $[f_{D2}/f_{D1}]_{I+II}$ ratio as a function of $\alpha (= N_{O,II}/N_{O,I})$ and $\beta (= P_{HDO,II}/P_{HDO,I})$ in the two stage model given by Equation (4) with $q = 0.25$. Above the dashed line ($\alpha\beta \gtrsim 1$), $[f_{D1}]_{I+II}$ is larger than $[f_{D1}]_I$ by a factor of two or more. See the text for more information.

ice mantle is expressed as

$$\left[\frac{f_{D2}}{f_{D1}} \right]_{I+II} \approx \frac{q(1+\alpha)(1+\alpha\beta^2)}{(1+\alpha\beta)^2}, \quad (4)$$

where α is $N_{O,II}/N_{O,I}$ and β is $P_{HDO,II}/P_{HDO,I}$. Figure 2 shows $[f_{D2}/f_{D1}]_{I+II}$ as a function of α and β with $q = 0.25$. It shows that the proposed scenario can lead to $[f_{D2}/f_{D1}]_{I+II} \gg 1$. The conditions to reproduce the observed values in NGC 1333-IRAS 2A, $HDO/H_2O \sim 10^{-3}$ and $(D_2O/HDO)/(HDO/H_2O) \sim 10$, are that 1) most of water ice is formed with $HDO/H_2O < 10^{-3}$ and that 2) an additional small amount ($\alpha < 0.1$) of highly fractionated ($\beta \gtrsim 100$) water ice is formed at later times.

Furuya et al. (2015, hereafter Paper I) studied the chemical evolution from H I dominated clouds to denser molecular clouds, following the scenario that H I dominated gas is swept up and accumulated by global accretion flows (e.g., Hartmann et al., 2001; Inoue & Inutsuka, 2012). Their primary goal was to investigate the evolution of the OPR(H₂) and the HDO/H₂O ratio without an arbitrary assumption concerning the initial OPR(H₂). It was found that the HDO/H₂O ratio in the bulk ice can be much lower

than 10^{-3} at the end of the main formation stage of H₂O ice, i.e., condition #1 can be satisfied. In the following, we conduct the gas-ice chemical simulations of collapsing prestellar cores to the formation of protostars in order to explore if condition #2 is fulfilled.

Based on the two stage model, we find that there are two regimes at the same $[f_{D2}/f_{D1}]_{I+II}$. Above the dashed line of Figure 2, where $\alpha\beta \gtrsim 1$, the difference between $[f_{D1}]_{I+II}$ and $[f_{D1}]_I$ is more than a factor of two, i.e., the HDO/H₂O ratio established at the main formation stage of H₂O ice is mostly hidden by water ice additionally formed at later times. Below the dashed line, on the other hand, $[f_{D1}]_{I+II}$ and $[f_{D1}]_I$ are similar. The former corresponds exactly to our scenario, where HDO and D₂O ices are predominantly formed after the main formation stage of H₂O ice. The latter is the case where H₂O and HDO ices are formed together, while D₂O ice is mainly formed after the main formation stage of H₂O and HDO ices. For the same $[f_{D2}/f_{D1}]_{I+II}$, the latter case requires more significant freeze out of oxygen, especially atomic oxygen and CO; water ice can be formed from CO gas through $CO + He^+ \rightarrow C^+ + O$. Which regime is more likely in the ISM, or in other words, does the HDO/H₂O ratio in the hot gas directly reflect the HDO/H₂O ice ratio at the main formation stage of H₂O ice? Numerical simulations are needed to answer the question.

3. Numerical Simulation

3.1. Model Description

We simulate water deuteration from a prestellar core to a protostellar core adopting one-dimensional radiation hydrodynamics simulations of Masunaga & Inutsuka (2000). Initially the core has an isothermal hydrostatic structure with a fixed outer boundary of 4×10^4 AU from the core center. The total mass of the core is $3.9 M_{\odot}$, which is greater than the critical mass for gravitational instability. The protostar is born at 2.5×10^5 yr after the beginning of the collapse, corresponding to $1.4 t_{ff}$, where t_{ff} is the free-fall time of the initial central density of hydrogen nuclei $\sim 6 \times 10^4 \text{ cm}^{-3}$. After the birth of the protostar, the model further follows the physical evolution for 9.3×10^4 yr.

Fluid parcels are traced in the hydrodynamics simulation, and we perform gas-ice chemical simulations along the stream lines to obtain the radial distribution of molecules in the protostellar envelope. This approach is the same as Aikawa et al. (2012). For simplicity, we set the temperature to be 10 K when the temperature in the original data is lower than 10 K. We adopt a rate equation method and the chemistry is described by a three-phase model, which consists of gas, a chemically active icy surface, and inert ice mantles (Hasegawa & Herbst, 1993b). The top four monolayers of ice mantles are assumed to be chemically active, following Vasyunin & Herbst (2013). We refer to all of the layers including both the ice surface and the inert ice mantle as the bulk ice mantle. We take into account gas-phase reactions, interaction between gas and (icy) grain surface, and surface reactions. For non-thermal desorption processes, we consider stochastic heating by cosmic-rays (Hasegawa & Herbst, 1993a), photodesorption (Westley et al., 1995), and chemical desorption (Garrod et al., 2007). Our chemical reaction network is originally based on Garrod & Herbst (2006). The network has been extended to include high-temperature gas-phase reactions from Harada et al. (2010), mono, doubly, and triply deuterated species (Aikawa et al., 2012; Furuya et al., 2013), and nuclear spin states of H₂, H₃⁺, and their isotopologues (Hincelin et al.,

Table 1. Initial Abundances of Selected Species with respect to Hydrogen Nuclei.

| Species | MC1 | MC2 | MC3 | AT1 | AT2 | AT4 |
|-------------------|----------|----------|----------|---------|---------|---------|
| o-H ₂ | 2.4(-2) | 1.1(-3) | 2.4(-4) | 4.5(-2) | 5.0(-3) | 5.0(-5) |
| p-H ₂ | 4.8(-1) | 5.0(-1) | 5.0(-1) | 4.5(-1) | 5.0(-1) | 5.0(-1) |
| HD | 1.4(-5) | 1.4(-5) | 1.1(-5) | 1.5(-5) | 1.5(-5) | 1.5(-5) |
| H I | 5.2(-4) | 7.3(-5) | 5.1(-5) | - | - | - |
| D I | 7.6(-7) | 9.5(-7) | 2.3(-6) | - | - | - |
| H ₂ O | 6.9(-9) | 5.2(-9) | 9.2(-9) | - | - | - |
| HDO | 1.2(-12) | 3.7(-11) | 1.3(-9) | - | - | - |
| D ₂ O | - | 2.9(-13) | 8.1(-11) | - | - | - |
| iH ₂ O | 8.4(-5) | 1.1(-4) | 1.2(-4) | - | - | - |
| iHDO | 1.1(-8) | 1.3(-8) | 3.4(-8) | - | - | - |
| iD ₂ O | 6.9(-13) | 7.1(-13) | 1.8(-11) | - | - | - |
| O I | 2.2(-5) | 1.7(-6) | 2.3(-7) | 1.8(-4) | 1.8(-4) | 1.8(-4) |
| O ₂ | 1.9(-9) | 4.0(-10) | 3.2(-10) | - | - | - |
| iO ₂ | - | - | - | - | - | - |
| CO | 6.1(-5) | 3.6(-5) | 5.1(-6) | - | - | - |
| iCO | 1.2(-5) | 3.1(-5) | 4.7(-5) | - | - | - |

Notes. $a(-b)$ means $a \times 10^{-b}$. o-H₂ indicates ortho-H₂, while p-H₂ indicates para-H₂. iX indicates species X in the bulk ice mantle. - indicates that abundances are less than 10^{-13} .

2014). The rate coefficients for the H₂ + H₃⁺ system are taken from Hugo et al. (2009). More details can be found in Paper I.

We consider six sets of the initial abundances for the collapse model, which are summarized in Table 1. In the sets labeled ‘MC’, the molecular abundances are adopted from Paper I. In Paper I, a one-dimensional shock model (Bergin et al., 2004; Hassel et al., 2010) was used to study the chemical evolution during the formation and growth of a molecular cloud via the accumulation of H I gas. Note that the evolution of the molecular cloud is dominated by ram pressure due to the accretion flow rather than self-gravity, which is in contrast with our collapse model. The time it takes for the column density of the cloud to reach $A_V = 1$ mag is ~ 4 Myr $(A_V/1 \text{ mag})(n_0/10 \text{ cm}^{-3})^{-1} (v_0/15 \text{ km s}^{-1})^{-1}$, where n_0 and v_0 are the preshock H I gas density and velocity of the accretion flow, respectively. The density and temperature of the molecular cloud are $\sim 10^4 \text{ cm}^{-3}$ and 10–15 K, respectively. We adopt the abundances when the column density of the molecular cloud reaches 1 mag (MC1), 2 mag (MC2), or 3 mag (MC3). In all three sets, H₂O ice is abundant ($x(\text{H}_2\text{Oice}) \sim 10^{-4}$, where $x(i)$ is the abundance of species i with respect to hydrogen nuclei) and the HDO/H₂O ice ratio is $\sim 10^{-4}$. On the other hand, the abundances of atomic oxygen and CO in the gas phase, and the OPR(H₂) vary by orders of magnitude among the three sets; all three values decrease with increasing the column density of the cloud. H₂ rather than CO is the key regulator of deuterium chemistry driven by $\text{H}_3^+ + \text{HD} \rightleftharpoons \text{H}_2\text{D}^+ + \text{H}_2$, as long as $\text{OPR}(\text{H}_2)/x(\text{CO}) \gtrsim 40$ at temperatures of $\lesssim 20$ K (Paper I). This condition is fulfilled in all three sets. The parameters α and β discussed in Section 2 are related to $(x(\text{CO}) + x(\text{O I}))$ and the OPR(H₂), respectively. In MC3, CO is largely frozen out, and its gas-phase abundance is only 5×10^{-6} . The observations of CO isotopologues toward the low-mass prestellar cores have found that the CO abundance in the gas phase is lower than the canonical value, $\sim 10^{-4}$, by a factor of around 10 (e.g., Crapsi et al., 2005). Then, the level of CO freeze out in MC3 is similar to that measured in prestellar cores. Although the physical parameters vary continuously as a function of time in our numerical simulation, it can be considered as a two stage model, since we connect the two different physical models, i.e., cloud formation and core collapse.

In previous studies of deuterium chemistry in collapsing cores, species were initially assumed to be in atomic form ex-

cept for H₂ and HD (e.g., Aikawa et al., 2012). For comparisons, we also perform chemical calculations in the collapsing core in which species are initially in atomic form except for H₂ and HD with the initial OPR(H₂) of 10^{-1} (AT1), 10^{-2} (AT2), or 10^{-4} (AT4).

The visual extinction at the outer edge of the core is set to be 5 mag, being irradiated by the Draine field (Draine, 1978). Paper I found that water ice deuteration can be significantly suppressed by interstellar UV radiation through the cycle of photodissociation and reformation of water ice, which efficiently removes deuterium from water ice chemistry. In this paper, our focus is placed on the water deuteration in the well-shielded regions. The cosmic-ray ionization rate of H₂ is set to be $1.3 \times 10^{-17} \text{ s}^{-1}$, while the flux of FUV photons induced by cosmic-rays is set to be $3 \times 10^3 \text{ cm}^{-2} \text{ s}^{-1}$. In these settings, photochemistry is not important for water ice.

Before the onset of the collapse, we assume that the prestellar core keeps its hydrostatic structure for some time. We consider three cases in which the elapsed time before the onset of the collapse is 0 yr (labeled ‘A’), 10^6 yr (corresponding to $5.6t_{\text{ff}}$, labeled ‘B’), or 3×10^6 yr ($16t_{\text{ff}}$, ‘C’). Our fiducial model is MC2B; i.e., the initial molecular abundance is set by the cloud formation model at the epoch when the column density reaches 2 mag, and the duration of the static prestellar phase is 10^6 yr.

3.2. Results

3.2.1. Fiducial model

Figure 3 shows the temporal variation of molecular abundances and abundance ratios in the fiducial model (MC2B) along the stream line of a fluid parcel. The fluid parcel is initially at 10^4 AU from the core center and finally reaches 5 AU. Figure 4 shows the fractional composition and the D/H ratios in the active surface ice layers in the fluid parcel as a function of the number of ice layers in total. Note that surface layers become part of the inert ice mantle with the growth of ice. Initially, most oxygen is locked up in CO and water ice with bulk ice ratios of HDO/H₂O and D₂O/HDO of $\sim 10^{-4}$. In the static phase and during the collapse at $T < 20$ K, the environment is favorable for deuteration: the low temperature, 10–20 K, and the relatively low OPR(H₂), $\sim 10^{-3}$, and the weak UV radiation field. During those periods,

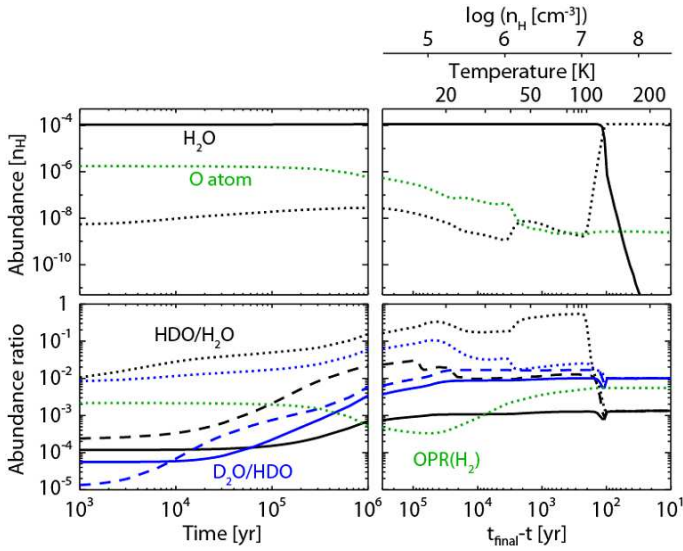


Fig. 3. Temporal variations of molecular abundances (top) and abundance ratios (bottom) in the static phase (left) and during the collapse (right) in model MC2B in the fluid parcel, which reaches $R = 5$ AU at the final time of the simulation. Before the collapse begins, the temperature is 10 K and the number density of hydrogen nuclei (n_{H}) is $2.3 \times 10^4 \text{ cm}^{-3}$. The horizontal axis of the right panels is set to be $t_{\text{final}} - t$, where t_{final} represents the final time of the simulation and $t = 0$ corresponds to the onset of the collapse. The solid lines, the dashed lines, and the dotted lines represent molecules in the bulk ice mantle, molecules in the surface ice layers, and gaseous molecules, respectively.

corresponding to layers ~ 70 -90 in Figure 4, a small amount of additional water ice (the total abundance of $\sim 5 \times 10^{-6}$) is formed with $\text{HDO}/\text{H}_2\text{O} > \text{D}_2\text{O}/\text{HDO} \gtrsim 10^{-2}$. The source of oxygen to form the water ice is gaseous atomic oxygen and CO. The additional water ice formation increases the concentrations of HDO and D_2O in the outer layers of the ice mantle, where CO and methanol are abundant as shown in Figure 4. The $\text{D}_2\text{O}/\text{HDO}$ ratio in the bulk ice becomes similar to that in the surface layers with time, while the $\text{HDO}/\text{H}_2\text{O}$ ratio in the bulk ice remains much lower than that in the surface layers due to the abundant H_2O in the inert ice mantle. The $\text{D}_2\text{O}/\text{HDO}$ ratio in the bulk ice becomes larger than the $\text{HDO}/\text{H}_2\text{O}$ ratio in 10^5 yr in the static phase.

The top panel of Figure 5 shows radial profiles of the abundances of H_2O , HDO and D_2O at 9.3×10^4 yr after the protostellar birth, while the lower panel shows radial profiles of the $\text{HDO}/\text{H}_2\text{O}$ and $\text{D}_2\text{O}/\text{HDO}$ ratios. The water sublimation radius, where the dust temperature is ~ 150 K, is located at around 60 AU from the protostar; water is mostly in the gas phase in the inner regions, while it predominantly exists as ice in the outer regions (Aikawa et al., 2012). At the water sublimation radius, both the gaseous $\text{HDO}/\text{H}_2\text{O}$ and $\text{D}_2\text{O}/\text{HDO}$ ratios drop via sublimation of ice. At $T \gtrsim 150$ K, the gaseous ratios directly reflect those in the bulk ice. At $T \lesssim 150$ K, the gaseous ratios are determined by ion-neutral chemistry in the gas phase; photodesorption is less important than the ion-neutral reactions, because of the weak UV radiation field dominated by the cosmic-ray induced UV. We confirmed that the gaseous $\text{HDO}/\text{H}_2\text{O}$ and $\text{D}_2\text{O}/\text{HDO}$ ratios in the outer regions do not reflect either those in the bulk ice or those in the surface layers. The model predicts $\text{HDO}/\text{H}_2\text{O} \sim 10^{-3}$ and $\text{D}_2\text{O}/\text{HDO} \sim 10^{-2}$ at $T \gtrsim 150$ K, which agree with the values measured in NGC 1333-IRAS

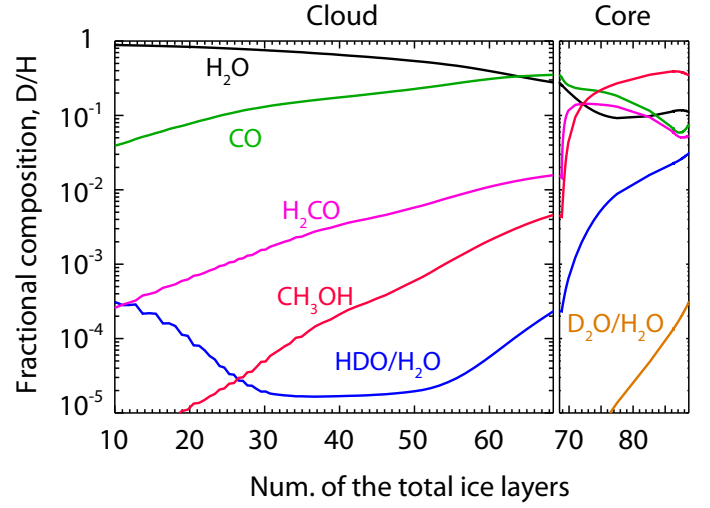


Fig. 4. Fractional composition and D/H ratios in the surface ice layers as functions of the total number of icy layers in model MC2B. The left panel represents the formation stage of a molecular cloud taken from Paper I, while the right panel represents the static and collapse stages at $t_{\text{final}} - t < 8.3 \times 10^4$ yr, where dust temperature is 10 K, in the same fluid parcel shown in Figure 3. The visual extinction for calculating photochemical rates increases from 2 mag at the end of the cloud formation stage to 5 mag at the prestellar core stage. The sudden increase leads to the sharp change of the fractional composition especially of H_2CO and CH_3OH in the surface ice layers.

2A (Coutens et al., 2014). Our simulations demonstrate that the combination of cold deuterium chemistry and sublimation of ice can account for observed features #1 and #2, i.e., the radial gradient of the gaseous $\text{HDO}/\text{H}_2\text{O}$ ratio and the higher $\text{D}_2\text{O}/\text{HDO}$ than $\text{HDO}/\text{H}_2\text{O}$ ratios in the inner hot regions, simultaneously.

In the fiducial model, the $\text{HDO}/\text{H}_2\text{O}$ gas ratio at $T > 150$ K is higher than the initial $\text{HDO}/\text{H}_2\text{O}$ ice ratio by a factor of 11. We denote this enhancement factor as ϵ_{D1} . The initial $\text{HDO}/\text{H}_2\text{O}$ ice ratio is mostly overshadowed by the small amount of highly fractionated water ice formed in the core. To check the dependence of the result on the initial $\text{HDO}/\text{H}_2\text{O}$ ice ratio, we also run another two models, in which the initial $\text{HDO}/\text{H}_2\text{O}$ ice ratio is artificially set to be 10^{-5} (MC2B-L) and 10^{-3} (MC2B-H), respectively. Other details are the same as in the fiducial model. In models MC2B-L and MC2B-H, ϵ_{D1} are 120 and 2, respectively. The differences in the $\text{HDO}/\text{H}_2\text{O}$ ratios, on the other hand, at $T > 150$ K among the three models MC2B, MC2B-L, and MC2B-H are within a factor of two, in spite of the difference in the initial $\text{HDO}/\text{H}_2\text{O}$ ice ratio by two orders of magnitude. Again it means that the initial $\text{HDO}/\text{H}_2\text{O}$ ice ratios are mostly overshadowed.

In our models, the main formation pathways of H_2O and HDO ices at $T < 20$ K are the surface reactions, $\text{OH} + \text{H}_2 \rightarrow \text{H}_2\text{O} + \text{H}$ and $\text{OD} + \text{H}_2 \rightarrow \text{HDO} + \text{H}$, respectively. Unexpectedly D_2O ice is formed via ion-neutral reactions in the gas phase followed by freeze out, instead of surface reactions. To check whether our results depend on the main formation pathways of water ice, we reran the fiducial model without the reaction $\text{OH} + \text{H}_2 \rightarrow \text{H}_2\text{O} + \text{H}$ and its deuterated analogues. In this case, the main formation pathways of water ice are barrierless reactions of atomic hydrogen/deuterium with OH/OD. We confirmed that the $\text{HDO}/\text{H}_2\text{O}$ and $\text{D}_2\text{O}/\text{HDO}$ ratios at $T > 150$ K are similar to the fiducial case; both ratios are enhanced by only $\sim 40\%$.

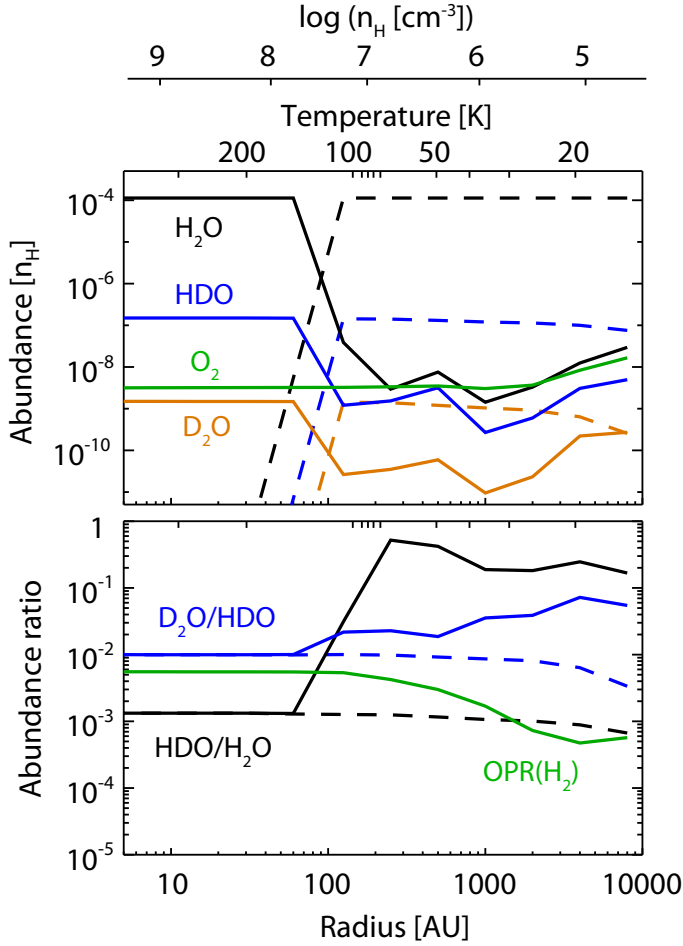


Fig. 5. Radial profile of the molecular abundances (upper panel) and the abundance ratios of the molecules (lower panel) in model MC2B at 9.3×10^4 yr after the protostellar birth. The labels at the top represent the temperature and density structures. The solid lines represent gaseous molecules, while the dashed lines represent icy molecules in the bulk ice mantle.

3.2.2. Grid of models

Table 2 summarizes the results from our grid of the models with variations in the initial abundances and the elapsed time before the onset of the collapse. In general, the models labeled MC predict a higher D_2O/HDO ratio than HDO/H_2O ratio at $T > 150$ K. Therefore, specific conditions are not necessary to reproduce the observed ratios in IRAS 2A. One exception is model MC1A, in which the initial $OPR(H_2)$ is high ($\sim 5 \times 10^{-2}$) and the collapse begins immediately. The time required for the $OPR(H_2)$ to reach steady state is longer than the free-fall timescale (Flower et al., 2006); the $OPR(H_2)$ is higher than 10^{-2} during the simulation, which reduces the efficiency of the overall deuteration processes, and prevents the enrichment of deuterated water in ice.

The enhancement factor of the HDO/H_2O ratio, ε_{D1} , is also listed in Table 2. In general, ε_{D1} is larger than 2 in models labeled MC. Therefore, the HDO/H_2O ice ratio established at the main formation phase of H_2O ice is mostly hidden by the additional formation of highly deuterated water ice at later times.

The models labeled AT tend to predict lower D_2O/HDO ratios than HDO/H_2O ratios at $T > 150$ K, in agreement with previous numerical studies (e.g., Aikawa et al., 2012). In these models, the gradient of deuterium fractionation seems not to be

large enough. This is due to the fact that the initial $OPR(H_2)$, which is treated as a free parameter, controls the overall deuteration processes, again because the time required for the $OPR(H_2)$ to reach steady state is longer than the free-fall timescale and the freeze-out timescale, i.e., the formation timescale of ice (Flower et al., 2006; Taquet et al., 2014). Note that the steady state value of the $OPR(H_2)$ for the initial dense core condition is of the order of 10^{-4} . With the low initial $OPR(H_2)$ of 10^{-4} , deuterium fractionation is already efficient at the main formation stage of H_2O ice, while with the high initial $OPR(H_2)$ of $\geq 10^{-2}$, the efficiency of the overall deuterium fractionation is reduced during the cold prestellar core phase. Among the models labeled AT, only models with a high initial $OPR(H_2)$ and a very long static phase (AT1C and AT2C) predict higher D_2O/HDO than HDO/H_2O ratios.

4. Discussion

4.1. O_2 and ortho-para ratio of H_2

In the simulations of the collapsing core, the critical parameters controlling the HDO/H_2O and D_2O/HDO ratios in the hot gas around protostars are the $OPR(H_2)$ and the amount of oxygen, i.e., atomic oxygen and CO, that is available for water ice formation. Here we briefly compare our model predictions with the observationally derived O_2 abundance and $OPR(H_2)$ toward low-mass protostars. Although the abundance of atomic oxygen in the cold outer envelopes is hard to constrain via observations, we can partly verify the oxygen chemistry in our models by comparing the predicted O_2 abundance with that derived from observations.

Yıldız et al. (2013) derived an upper limit of O_2 gas abundance $\lesssim 10^{-8}$ toward NGC 1333-IRAS 4A, assuming a constant abundance in the envelope. Brünken et al. (2014) derived the $OPR(H_2D^+)$ of ~ 0.1 in the cold outer envelope of IRAS 16293-2422, which corresponds to an $OPR(H_2)$ of 2×10^{-4} in their best fit model. In general, the models which predict a higher D_2O/HDO than HDO/H_2O ratio in the gas phase at $T > 150$ K reproduce the observations of O_2 and $OPR(H_2)$ better than the other models. Our fiducial model, for example, is consistent with the upper limit of the O_2 abundance and the $OPR(H_2)$ derived from the observations, as shown in Figure 5 and Table 2. Unless a very long static phase ($16t_{ff}$) is assumed, the models labeled AT tend to overpredict the O_2 abundance, implying that the majority of oxygen should be locked up in molecules such as water and CO before the prestellar core stage (Yıldız et al., 2013; Bergin et al., 2000).

In summary, our models labeled MC reasonably reproduce the observations of the water deuterium fractionation, the O_2 abundance, and the $OPR(H_2)$, simultaneously. This strengthens our scenario. Note, however, that these observed values are measured in different sources, and it is unclear whether the higher D_2O/HDO ratio compared with HDO/H_2O , the low O_2 abundance, and the low $OPR(H_2)$ are general chemical features of low-mass protostellar sources.

4.2. Water deuteration versus Methanol deuteration

In the inner hot regions ($T \gtrsim 100$ K) of low-mass protostellar sources, formaldehyde and methanol show higher levels of deuterium fractionation than water. For example, the CH_3OD/CH_3OH ratio ($\gtrsim 10^{-2}$; Parise et al., 2006) is much higher than the HDO/H_2O ratio ($\sim 10^{-3}$; e.g., Persson et al., 2014). This difference is thought to reflect the different epoch of

Table 2. Summary of Model Results

| Model | H ₂ O ^a | HDO ^b | | D ₂ O ^b | | ε_{D1}^c | CH ₃ OH ^b | | O ₂ ^d | OPR(H ₂) ^e |
|--------|-------------------------------|------------------|---------|-------------------------------|----------------------|----------------------|---------------------------------|--------------------|-----------------------------|-----------------------------------|
| | | H ₂ O | HDO | HDO | HDO/H ₂ O | | H ₂ O | CH ₃ OH | | |
| MC1A | 9.8(-5) | 2.8(-4) | 2.4(-4) | 0.8 | 2.2 | 7.8(-2) | 3.4(-4) | 4.1(-7) | 3.1(-2) | |
| MC1B | 1.0(-4) | 6.0(-4) | 2.1(-3) | 3.5 | 4.6 | 2.2(-1) | 6.4(-4) | 7.6(-8) | 3.7(-3) | |
| MC2A | 1.1(-4) | 5.8(-4) | 4.1(-3) | 7.2 | 4.8 | 4.8(-2) | 4.0(-3) | 2.7(-8) | 1.5(-3) | |
| MC2B | 1.1(-4) | 1.3(-3) | 1.0(-2) | 7.5 | 11 | 1.5(-1) | 6.1(-3) | 1.6(-8) | 4.7(-4) | |
| MC3A | 1.2(-4) | 7.1(-4) | 1.3(-2) | 19 | 2.5 | 2.5(-2) | 1.1(-2) | 4.9(-9) | 3.4(-4) | |
| MC3B | 1.2(-4) | 9.5(-4) | 1.6(-2) | 17 | 3.4 | 4.3(-2) | 1.4(-2) | 1.9(-9) | 2.5(-4) | |
| AT1B | 1.2(-4) | 6.7(-4) | 2.5(-4) | 0.4 | - | 7.5(-2) | 2.9(-4) | 7.8(-7) | 1.4(-2) | |
| AT1C | 1.2(-4) | 1.3(-3) | 1.0(-2) | 7.8 | - | 1.2(-1) | 2.5(-3) | 9.3(-9) | 3.0(-4) | |
| AT2B | 1.2(-4) | 2.4(-3) | 1.3(-3) | 0.6 | - | 7.4(-2) | 2.0(-3) | 7.8(-7) | 2.2(-3) | |
| AT2C | 1.2(-4) | 3.2(-3) | 6.3(-3) | 2.0 | - | 1.2(-1) | 5.0(-3) | 9.3(-9) | 2.8(-4) | |
| AT4B | 1.1(-4) | 6.4(-3) | 2.5(-3) | 0.4 | - | 7.2(-2) | 5.9(-3) | 7.8(-7) | 5.4(-4) | |
| AT4C | 1.2(-4) | 7.0(-3) | 4.2(-3) | 0.6 | - | 1.2(-1) | 7.9(-3) | 9.3(-9) | 2.7(-4) | |
| MC2B-L | 1.1(-4) | 1.2(-3) | 1.0(-2) | 8.8 | 120 | 1.5(-1) | 6.1(-3) | 1.6(-8) | 4.7(-4) | |
| MC2B-H | 1.1(-4) | 2.1(-3) | 6.1(-3) | 2.8 | 2.1 | 1.5(-1) | 6.1(-3) | 1.6(-8) | 4.7(-4) | |

Notes. Values at 9.3×10^4 yr after the protostellar birth.

^(a) The abundance of H₂O gas with respect to hydrogen nuclei at $T > 150$ K. ^(b) Abundance ratios at $T > 150$ K. ^(c) The ratio of the gaseous HDO/H₂O ratio at $T > 150$ K to the initial HDO/H₂O ice ratio. ^(d) The maximum abundance of O₂ gas with respect to hydrogen nuclei at $T < 150$ K. ^(e) The minimum ortho-to-para nuclear spin ratio of H₂ at $T < 150$ K.

their formation, i.e., water ice is formed in an earlier stage of star formation than formaldehyde and methanol ices (Cazaux et al., 2011; Taquet et al., 2012). Note that the scenario implicitly assumes that H₂O and HDO ices are formed at the same evolutionary stage.

In our scenario, H₂O ice is mainly formed in molecular clouds, while HDO and D₂O ices are mainly formed at later times when CO and methanol are the main constituent of the surface layers of the ice. In other words, H₂O ice is formed in an earlier stage of star formation than deuterated water, formaldehyde and methanol ices. This naturally leads to the following relation for the abundance ratios, CH₃OD/CH₃OH \sim D₂O/HDO $>$ H₂O/HDO, simply because methanol and deuterated water are formed at the similar epoch. The CH₃OD/CH₃OH ratios at $T > 150$ K in our grid of models are presented in Table 2 with the CH₃OH/H₂O ratios. Our fiducial model, for example, predicts CH₃OD/CH₃OH = 6×10^{-3} , D₂O/HDO = 1×10^{-2} , and HDO/H₂O = 1×10^{-3} , which agree reasonably well with the observations. Here we considered only the CH₃OD/CH₃OH ratio, since the ratio is determined by hydrogenation/deuteration of CO on a icy grain surface. Other species, such as HDCO and CH₂DOH, are subject to the abstraction and substitution reactions (Watanabe & Kouchi, 2008), and the situation is more complex (see Taquet et al., 2012, for a detailed discussion).

4.3. Thermally induced H-D exchange reactions

Laboratory experiments have shown that thermally activated H-D exchanges between hydrogen-bonded molecules in mixed ices occur efficiently at warm temperatures of ≥ 70 K (Ratajczak et al., 2009; Faure et al., 2015; Lamberts et al., 2015). This type of reactions is not included in our chemical network. In particular for the present study, Lamberts et al. (2015) experimentally studied the thermally activated H-D exchange reactions,



in mixed amorphous ices. In equilibrium, the ratio of the D₂O/HDO ratio to the HDO/H₂O ratio is given as k_{5b}/k_{5f} , where k_{5b} and k_{5f} are the reaction rate coefficient of Reaction

(5) in the backward direction and the forward direction, respectively. Lamberts et al. found that the activation energy barrier of the forward reaction is 3840 ± 125 K, which is much smaller than the binding energy of water on a water substrate, 5700 K (Fraser et al., 2001). Although the activation barrier for the backward reaction has not been measured in laboratory, the backward reaction is energetically less favorable than the forward reaction, i.e., likely $k_{5b}/k_{5f} < 1$ (Collier et al., 1984; Lamberts et al., 2015). Taken together, the D₂O/HDO ice ratio can be lowered during the warm-up of ices in in-falling protostellar envelopes (Lamberts et al., 2015).

To check the impact of the H-D exchange by Reaction (5), we compared the timescale of forward reaction calculated by Lamberts et al. (2015) and the duration time of the warm temperatures in our collapse model, and found that the former is much shorter than the latter at ≥ 80 K. Then D₂O in ice would be largely lost prior to the sublimation of water ice, if Reaction (5) is as efficient in the ISM as in laboratory. This challenges the D₂O observations by Coutens et al. (2014), who showed that the D₂O emission peak is located at the peak of the continuum emission as well as the H₂¹⁸O and the HDO emissions.

A possible explanation for the discrepancy is the layered ice structure in the ISM. Ratajczak et al. (2009) experimentally demonstrated that thermally activated H-D exchange between CD₃OD and H₂O occurs efficiently in mixed ice at $T > 120$ K, while the exchange does not occur in the case of segregated ice even at higher temperatures on a laboratory timescale. As noted in Ratajczak et al. (2009), this implies that the H/D exchange occurs only between closely interacting molecules in ice. In the experiments by Lamberts et al. (2015), mixed ices with the mixing ratio of (H₂O:D₂O) \sim (1:1) were used, which ensures that each D₂O has at least one neighbour of H₂O. In our scenario, however, D₂O is mainly present in the CO/CH₃OH-rich outer-layers, i.e., significant fraction of D₂O would not be neighbored by H₂O molecules, and it may be the limiting factor of the H/D exchange by Reaction (5) in the ISM.

5. Conclusion

Recent interferometer observations have found that the D₂O/HDO ratio is higher than the HDO/H₂O ratio in the warm gas surrounding the low-mass protostar NGC 1333-IRAS 2A, where water ice has sublimated (Coutens et al., 2014). In this study, we have proposed that the observed feature is a natural consequence of chemical evolution in the early cold stages of low-mass star formation: 1) majority of oxygen is locked up in water ice and other molecules in molecular clouds, where water deuteration is not efficient, and 2) water ice formation continues with much reduced efficiency in cold prestellar/protostellar cores, where deuteration processes are highly enhanced. Using a simple analytical model and gas-ice astrochemical simulations on the formation of molecular clouds (Paper I) and the gravitational collapse of dense cores, we have shown that the scenario can quantitatively explain the HDO/H₂O ratio and the D₂O/HDO ratio measured in IRAS 2A. Our model predictions are consistent with the low abundance of O₂, the low OPR(H₂), and the CH₃OD/CH₃OH ratio measured in low-mass protostellar sources, which further supports the scenario. We also found that the majority of HDO and D₂O ices are likely formed in cold prestellar/protostellar cores rather than in molecular clouds, where the majority of H₂O ice is formed. Considering the layered ice mantles, this implies that HDO and D₂O are predominantly present in the CO/CH₃OH-rich outer layers of ice mantles rather than in the H₂O-dominated inner layers. The layered ice structure indicates that the gaseous HDO/H₂O ratio produced by photodesorption *does not* reflect that of the bulk ice (see also Taquet et al., 2014).

The present study demonstrates the power of the combination of the HDO/H₂O and D₂O/HDO ratios as a tool to reveal the past history of water ice formation in the early cold stages of star formation and when the enrichment of deuterium in the bulk of water occurred. Further observations are desirable to investigate if the relation, D₂O/HDO > HDO/H₂O, is common in low-mass protostellar sources.

Acknowledgements. We thank Magnus V. Persson, Thanja Lamberts, Vianney Taquet, Catherine Walsh, and Maria N. Drozdovskaya for interesting discussions. We also thank the referee for his/her comments. Astrochemistry in Leiden is supported by the Netherlands Research School for Astronomy (NOVA), by a Royal Netherlands Academy of Arts and Sciences (KNAW) professor prize, and by the European Union A-ERC grant 291141 CHEMPLAN. K.F. is supported by the Research Fellowship from the Japan Society for the Promotion of Science (JSPS). Numerical computations were in part carried out on PC cluster at Center for Computational Astrophysics, National Astronomical Observatory of Japan.

References

Aikawa, Y., Wakelam, V., Hersant, F., Garrod, R., & Herbst, E. 2012, *ApJ*, 760, 40
 Allen, M., & Robinson, G. W. 1977, *ApJ*, 212, 396
 Bergin, E. A., Hartmann, L. W., Raymond, J. C., & Ballesteros-Paredes, J. 2004, *ApJ*, 612, 921
 Bergin, E. A., Melnick, G. J., Stauffer, J. R., et al. 2000, *ApJ*, 539, L129
 Boogert A., Gerakines P., & Whittet D., 2015, *ARA&A*, 53, 541
 Brünken, S., Sipilä, O., Chambers, E. T. et al. 2014, *Nature*, 516, 219
 Butner, H. M., Charnley, S. B., Ceccarelli, C., et al. 2007, *ApJ*, 659, L137
 Caselli, P., & Ceccarelli, C. 2012, *ARA&A*, 20, 56
 Caselli, P., Keto, E., Bergin, E. A., et al. 2012, *ApJ*, 759, L37
 Cazaux, S., Caselli, P., & Spaans, M. 2011, *ApJ*, 741, L34
 Ceccarelli, C., Caselli, P., Bockelée-Morvan, D., Mousis, O., Pizzarello, S., Robert, F. & Semenov, D. 2014, *Protostars & Planets VI* (Tucson: Univ. Arizona Press), 859
 Collier W. B., Ritzhaupt G., & Devlin J. P., 1984, *J. Phys. Chem.*, 88, 363
 Coutens, A., Vastel, C., & Caux, E., et al. 2012, *A&A*, 539, 132
 Coutens, A., Vastel, C., Cabrit, S., et al. 2013, *A&A*, 560, 39
 Coutens, A., Jørgensen, J. K., Persson, M., et al. 2014, *ApJ*, 792, L5

Crapsi, A., Caselli, P., Walmsley, C. M., et al. 2005, *ApJ*, 619, 379
 Dartois, E., Thi, W. F., Geballe, T. R., et al. 2003, *A&A*, 399, 1020
 Draine, B. T. 1978, *ApJS*, 36, 595
 Faure, M., Quirico, E., Faure, A., Schmitt, B., Theulé, P., & Marboeuf, U. 2015, *Icarus*, 261, 14
 Flower, D. R., Pineau Des Forêts, G., Walmsley, C. M. 2006, *A&A*, 449, 621
 Furuya, K., Aikawa, Y., Nomura, H., Hersant, F., & Wakelam, V. 2013, *ApJ*, 779, 11
 Furuya, K., Aikawa, Y., Hincelin, U., Hassel, G. E., Bergin, E. A., Vasyunin, A. I., & Herbst, E. 2015, *A&A*, 584, 124
 Fraser, H. J., Collings, M. P., McCoustra, M. R. S., & Williams, D. A. 2001, *MNRAS*, 327, 1165
 Garrod, R. T., & Herbst, E. 2006, *A&A*, 457, 927
 Garrod, R. T., Wakelam, V., & Herbst, E. 2007, *A&A*, 467, 1103
 Harada, N., Herbst, R., & Wakelam, V. 2010, *ApJ*, 721, 1570
 Hartmann, L., Ballesteros-Paredes, J., & Bergin, E. A. 2001, *ApJ*, 562, 852
 Hasegawa, T. I., & Herbst, E. 1993, *MNRAS*, 261, 83
 Hasegawa, T. I. & Herbst, E. 1993, *MNRAS*, 263, 589
 Hassel, G. E., Herbst, E., & Bergin, E. A. 2010, *A&A*, 515, 66
 Hincelin, U., Herbst, E., Chang, Q., Vasyunina, T., Aikawa, Y., & Furuya, K. 2014, 69th International Symposium on Molecular Spectroscopy, 9
 Hugo, E., Asvany, O. & Schlemmer, S. 2009, *J. of Chem. Phys.*, 130, 164302
 Inoue, T., & Inutsuka, S. 2012, *ApJ*, 759, 35
 Ioppolo, S., Cuppen, H. M., Romanzin, C., van Dishoeck, E. F., & Linnartz, H. 2008, *ApJ*, 686, 1474
 Jørgensen, J. K., & van Dishoeck, E. F. 2010, *ApJ*, 725, L172
 Lamberts, T., Ioppolo, S., Cuppen, H. M., Fedoseev, G., & Linnartz, H. 2015, *MNRAS*, 448, 3820
 Linsky, J. L. 2003, *Space Sci. Rev.*, 106, 49
 Liu, F.-C., Parise, B., Kristensen, L., Visser, R., van Dishoeck, E. F., & Güsten, R. 2011, *A&A*, 527, 19
 Masunaga, H., & Inutsuka, S. 2000, *ApJ*, 531, 350
 Miyauchi, N., Hidaka, H., Chigai, T., et al. 2008, *Chem. Phys. Lett.*, 456, 27
 Mokrane, H., Chaabouni, H., Accolla, M., et al. 2009, *ApJ*, 705, L195
 Nagaoka, A., Watanabe, N., Kouchi, A. 2005, *ApJ*, 624, L29
 Oba, Y., Watanabe, N., Hama, T., Kuwahata, K., Hidaka, H., & Kouchi, A. 2012, *ApJ*, 749, 67
 Oba, Y., Osaka, K., Watanabe, N., Chigai, T., & Kouchi, A. 2014, *Faraday Disc.*, 168, 185
 Öberg, K. I., Boogert, A. C. A., Pontoppidan, K. M., et al. 2011, *ApJ*, 740, 109
 Paganí, L., Olofsson, A. O. H., Bergman, P., et al. 2003, *A&A*, 402, L77
 Parise, B., Simon, T., Caux, E., et al. 2003, *A&A*, 410, 897
 Parise, B., Ceccarelli, C., Tielens, A. G. G. M., Castets, A., Caux, E., Lefloch, B. & Maret, S. 2006, *A&A*, 453, 949
 Persson, M. V., Jørgensen, J. K., & van Dishoeck, E. F. 2013, *A&A*, 549, L3
 Persson, M. V., Jørgensen, J. K., van Dishoeck, E. and Harsono, D. 2014, *ApJ*, 563, 74
 Pontoppidan, K. M. 2006, *A&A*, 453, L47
 Ratajczak, A., Quirico, E., Faure, A., Schmitt, B., & Ceccarelli, C. 2009, *A&A*, 496, L21
 Rodgers, S. D., & Charnley, S. B. 2002, *Planet. Space Sci.*, 50, 1125
 Taquet, V., Ceccarelli, C. & Kahane, C. 2012, *ApJ*, 748, L3
 Taquet, V., López-Sepulcre, A., Ceccarelli, C., et al. 2013, *ApJ*, 768, L29
 Taquet V., Charnley S. B., Sipilä O., 2014, *ApJ*, 791, 1
 Tielens, A. G. G. M. 2005, *The Physics and Chemistry of the Interstellar Medium* (Cambridge: Cambridge Univ. Press), 219
 van Dishoeck, E. F., Bergin, E. A., Lis, D. C., & Lunine, J. I. 2014, *Protostars & Planets VI* (Tucson: Univ. Arizona Press), 835
 Vasyunin, A. I. & Herbst, E. 2013, *ApJ*, 762, 86
 Wakelam, V., Vastel, C., Aikawa, Y., Coutens, A., Bottinelli, S. & Caux, E. 2014, *MNRAS*, 445, 2854
 Watanabe, N., & Kouchi, A. 2008, *Prog. Surf. Sci.*, 83, 439
 Westley, M. S., Baragiola, R. A., Johnson, R. E., & Baratta, G. A. 1995, *Nature*, 373, 405
 Whittet, D. C. B. 1993, *Dust and Chemistry in Astronomy* (Bristol and Philadelphia: Institute of Physics Publishing), 9
 Yıldız, U. A., Acharyya, K., Goldsmith, P. F. et al. 2013, *A&A*, 558, 58